Large-amplitude nuclear motions in the laser-induced Coulomb explosion of carbon dioxide molecules

C. Cornaggia
Commissariat à l'Energie Atomique, Division des Sciences de la Matière, Service des Photons, Atomes et Molécules, Bâtiment 522, F-91191 Gif-sur-Yvette, France
(Received 26 June 1995)

Intense femtosecond laser pulses are used to study the Coulomb explosion of CO_2 molecules via $O^{Z''+}+C^{Z'+}+O^{Z+}$ fragmentation channels. Large-amplitude bending and stretching motions around an average linear elongated structure are observed using atomic ion momenta correlations' peak shapes in comparison with Coulomb explosion calculations. Of special interest are the enhanced multielectronic ionization at large internuclear separations as predicted by recent theoretical models developed for diatomic molecules and the strong structural transition between the unperturbed geometry of the molecule and the exploding configuration in the intense laser field. [S1050-2947(96)50610-4]

PACS number(s): 33.80.Rv;33.80.Eh;42.50.Vk

Laser-induced Coulomb explosion experimental studies performed on small polyatomic species such as CO_2 or C_2H_2 have shown that the multifragmentation following the ejection of valence electrons is a direct process without any formation of intermediate daughter molecular ions [1,2]:

$$[ABC^{M+}]\rightarrow A^{Z''+}+B^{Z'+}+C^{Z+}+(\text{kinetic-energy release}), \quad (1)$$

where $[ABC^{M+}]$ represents a transient triatomic multicharged ion and $A^{Z''+}$, $B^{Z'+}$, and C^{Z+} the multicharged atomic ions. The Coulomb explosion terminology is used because of the instantaneous character of the multifragmentation, and the fact that the charge separation is dominated by Coulomb repulsion forces yielding high atomic ion energies. However, for molecules built with light atomic elements H, C, N, and O, the measured total kinetic-energy releases are found to be 50% weaker than the kinetic-energy releases expected from a pure Coulomb repulsion of pointlike charges starting at the molecular equilibrium internuclear distances. Due to the $Z'Z/R$ dependence of the Coulomb repulsion potential where R represents the nuclear coordinates, a simple interpretation is to assume that the molecule is strongly perturbed by the intense laser field and explodes at twice its equilibrium internuclear distances. This hypothesis has been confirmed by recent theoretical models, which predict a dramatic enhancement of multiple ionization and subsequent Coulomb explosion at critical internuclear distances larger than the equilibrium distances of the unperturbed molecule [3–6].

This experimental work shows that a wide nuclear range exists for the predicted enhancement of multi-ionization. Within this range, large-amplitude bending and stretching motions take place during the molecular explosion. The experimental procedure allows one to get the different components of the atomic ions' momenta using the molecular orientation along the laser polarization axis. The covariance mapping technique produces peak shapes in two- or three-dimensional mass spectra, which represent momenta correlations of the departing atomic ions [7]. Then, the obtained experimental results are compared to momenta calculations which include bent and stretched geometrical configurations of the molecule for the initial atomic positions.

The molecular Coulomb explosion is produced by a 130-fs Ti:sapphire laser system operating at $\lambda=790$ nm and focused intensities up to 2×10^{16} W/cm^2 (CEA/DRECAM laser facility), and is analyzed using a Wiley and McLaren short time-of-flight ion spectrometer [8]. Figures 1 and 2 show double-correlation maps recorded with CO_2 when the laser polarization direction is respectively parallel and perpendicular to the detection axis. Time-of-flight spectra are plotted as curves to the bottom and left with respectively horizontal T_1 and vertical T_2 time-of-flight axes, which are used for the representation of the $R^{(2)}(T_1,T_2)$ correlation coefficient. In the parallel configuration (Fig. 1) the oxygen

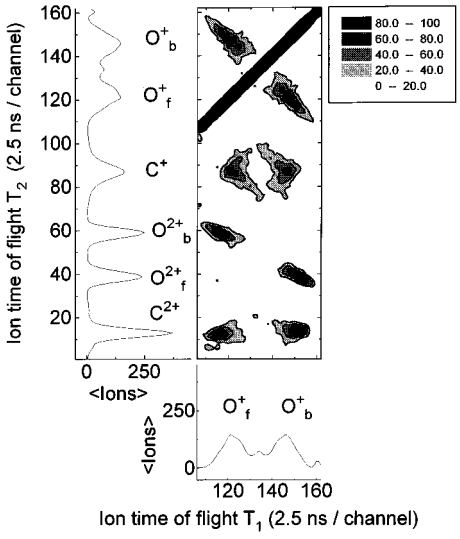

FIG. 1. Double-correlation map of CO_2 recorded at $\lambda=790$ nm and $I=10^{15}$ W/cm^2 with the laser polarization direction parallel to the detection axis. The correlation coefficient $R^{(2)}(T_1,T_2)$ is multiplied by 1000 and is represented using a five-level gray scale as a function of the T_1 (horizontal axis) and T_2 (vertical axis) ion times of flight.

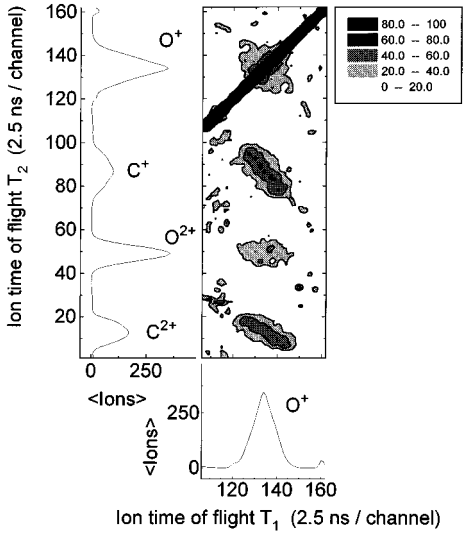

FIG. 2. Double-correlation map of CO_2 recorded at $\lambda=790$ nm and $I=10^{15}$ W/cm^2 with the laser polarization direction perpendicular to the detection axis.

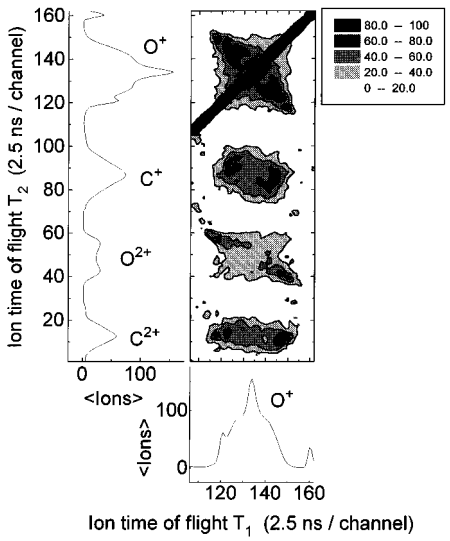

FIG. 3. Double-correlation map of CO_2 recorded at $\lambda=790$ nm and $I=10^{15}$ W/cm^2 with circular laser polarization.

ions are ejected toward and away from the detector (forward $O^{Z'+}{}_f$ and backward $O^{Z+}{}_b$ ions) and present a double-peak structure, while the middle carbon ions produce a single-peak shape. In the perpendicular case (Fig. 2) the time-of-flight spectrum exhibits oxygen and carbon ion peaks with comparable widths, which constitute first hints of bending motions, since a stiff exploding molecule would produce narrower carbon peaks. For the sake of clarity, only double correlations involving the O^+ ion are presented and analyzed throughout this Rapid Communication. The correlation maps in Figs. 1 and 2 exhibit a variety of correlation peak shapes. In Fig. 1, the C^+-O^+ correlation peaks look like corners of a parallelogram corresponding to correlations of the C^+ ion with the forward ($O^+{}_f$) and backward($O^+{}_b$) components of the O^+ ions. In the perpendicular configuration illustrated in Fig. 2, only a single peak appears in the middle of the above-mentioned parallelogram. The same physical event detected in parallel and perpendicular configurations shows the complementarity of the experimental data. In fact, the degeneracy of the ion momenta measurements can be overcome by performing experiments at different molecular orientations. Finally, Fig. 3 represents the correlation map recorded with circular polarization for which the molecular explosion can be considered as isotropic in space. The C^+-O^+ correlation peak is now the whole parallelogram, since all the components of the momenta along the spectrometer axis are detected.

The observed correlation peak shapes are reproduced following a two-step approach. The first step is to perform Coulomb explosion calculations in the molecular frame using a repulsive Coulomb potential:

$$V[\{\mathbf{R}_i\}_{i=1,n}]=\sum_{i<j} Z_jZ_i/|\mathbf{R}_j-\mathbf{R}_i|, \tag{2}$$

where $\{\mathbf{R}_i\}_{i=1,n}$ represent the vector positions of the n repelling atomic ions. Since the molecular ion kinetic energy before the explosion is negligible compared to the Coulomb repulsion energy, the initial positions determine the atomic ions' final momenta $\{\mathbf{P}_i\}_{i=1,n}$ at the end of the explosion. For each $O^{Z''+}+C^{Z'+}+O^{Z+}$ channel, the calculated momenta $\mathbf{P}_i$ are represented in the molecular frame by their modulii $P_i(\alpha,R)$ and angles $\beta_i(\alpha,R)$ with the Z axis as functions of the α angle between the C-O direction and the Z axis and the $R=R$(C-O) internuclear distance. The O-C-O angle is then $\pi-2\alpha$ and bent geometries are introduced with nonzero α values.

The second step is to calculate the momenta in the laboratory frame $P_d=\mathbf{e}_d\cdot\mathbf{P}$, where the unit vector $\mathbf{e}_d$ is parallel to the ion spectrometer axis. In the frame attached to the laser field, the orientation process does not change the initial isotropic azimuthal angle distribution $D_\phi(\phi)$ of the molecular frame, but produces a polar angle distribution $D_\theta(\theta)$ strongly peaked along the laser electric field. Deviations from the molecular linear configuration are introduced by the calculated β angles of the momentum $\mathbf{P}$ with the Z axis of the molecular frame. The measured P_d component of the momentum $\mathbf{P}$ is given by

$$P_d=P(\alpha,R)\{\cos(\theta_{pd})\cos[\theta+\beta(\alpha,R)] - \sin(\theta_{pd})\sin[\theta+\beta(\alpha,R)]\sin(\phi)\}, \tag{3}$$

where the angle θ_{pd} between the spectrometer and laser polarization axes is fixed by the experimental conditions. For a quantitative study, the nuclear coordinate distributions $D_\alpha(\alpha)$ and $D_R(R)$ and the orientation $D_\theta(\theta)$ of the molecular frame are introduced as symmetric triangular distributions. These distributions are respectively peaked at the observed average values $\alpha_c=0°$, $R_c=2R_e$(C-O), and $\theta_c=0°$, with half width at half maximum (HWHM) $\Delta\alpha_{1/2}$, $\Delta R_{1/2}$, and $\Delta\theta_{1/2}$, where R_e(C-O) is the internuclear distance of the C—O bond of the unperturbed CO_2 molecule.

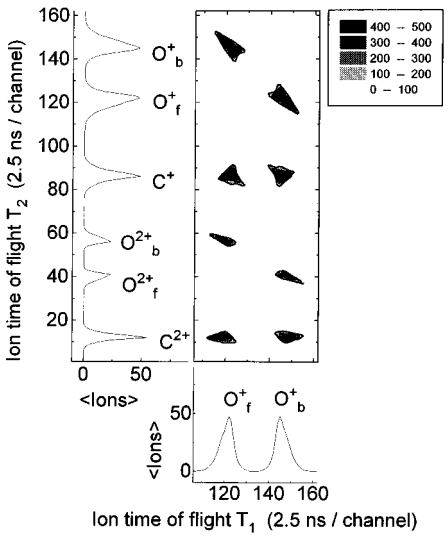

FIG. 4. Calculated double-correlation map with CO_2 molecules oriented along the detection axis and associated with the experimental data of Fig. 1.

Figures 4 and 5 represent the calculated double-correlation spectra that correspond respectively to the experimental results of Figs. 1 and 2. The molecular parameters $\Delta\alpha_{1/2}$, $\Delta\theta_{1/2}$, and $\Delta R_{1/2}$ remain the same for both calculations, while $\theta_{pd}=0°$ in the parallel case (Figs. 1 and 4) and $\theta_{pd}=90°$ in the perpendicular case (Figs. 2 and 5). The overall shapes of the correlation peaks are reproduced for each laser polarization, and several sets of parameters are tried until a good agreement is found between the experimental data and the calculations. Using an isotropic distribution $D_\theta(\theta)$ for the circular polarization, the calculated correlation peak shapes are again in good agreement with the experimental data of Fig. 3. In consequence, the numbers reported in Table I show clear evidence for large-amplitude stretching motions between $R_{\min}=R_e$(C-O) to $R_{\max}=3R_e$(C-O) and

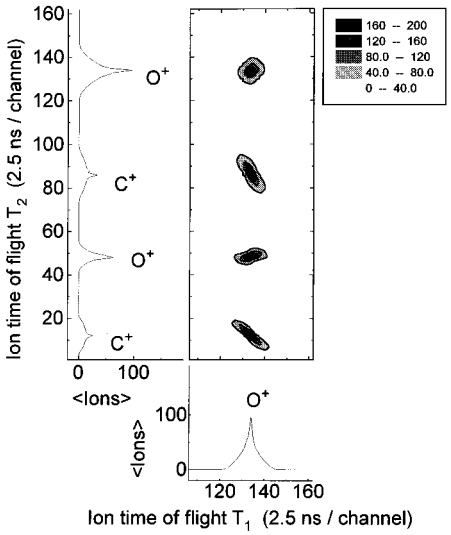

FIG. 5. Calculated double-correlation map with CO_2 molecules oriented perpendicular to the detection axis and associated with the experimental data of Fig. 2.

TABLE I. Molecular orientation HWHM $\Delta\theta_{1/2}$ around $\theta_c=0°$, angle HWHM $\Delta\alpha_{1/2}$ around $\alpha_c=0°$, and internuclear distance HWHM $\Delta R_{1/2}$ around $R_c=2R_e$(C-O) used in the calculations of correlation peaks for each detected channel $O^{Z''+}+C^{Z'+}+O^{Z+}$. The angles are in degrees and the $\Delta R_{1/2}$ values are in units of R_e(C-O)=1.16 Å, which is the C—O bond internuclear distance of the unperturbed CO_2 molecule in its ground electronic state.

Z'',Z',Z	$\Delta\theta_{1/2}$ (degrees)	$\Delta\alpha_{1/2}$ (degrees)	$\Delta R_{1/2}/R_e$(C-O)
1,1,1	30	20	0.5
1,2,1	20	20	0.5
2,2,1	20	20	0.5
2,2,2	15	20	0.5

bending motions up to $\alpha_{\max}=2\Delta\alpha_{1/2}=40°$, which constitute the most striking feature of this paper. For values $\Delta R_{1/2}$ and $\Delta\alpha_{1/2}$ corresponding to the zero-point vibration of the unperturbed molecule, the calculations cannot reproduce in any way the observed correlation maps. For the four introduced channels, the orientation of the molecular frame represented by the HWHM $\Delta\theta_{1/2}$ of the $D_\theta(\theta)$ distribution is more and more peaked around $\theta_c=0°$ as the number of removed electrons is increased.

The origin of these observed nuclear motions comes from physical processes such as the strong laser-induced electronic polarizability and multielectronic ionization. The laser-induced electronic polarizability involves bound and freed electrons from the molecular-ion core. The Coulomb interaction between the displaced bound or freed electrons and the nuclei will produce additional stretching and bending forces with an overall torque applied on the nuclear structure. Since the electronic oscillations are much faster than the nuclei motions, the nuclear potentials will exhibit an additional laser-induced potential term where the ponderomotive potential $U_p=e^2E^2/(4m_e\omega^2)$ should play a determinant role, as in the laser-atom interaction [9,10]. For the multielectronic ionization source of nuclear motions, recent models based respectively on field ionization [3] and nonperturbative time-dependent calculations [4–6] have predicted that multiple ionization and subsequent Coulomb explosion are dramatically enhanced for elongated nuclear coordinates. This experimental work shows that there exists a wide nuclear range for the predicted enhancement of multi-ionization, from R_e(C-O) to $3R_e$(C-O) for the C—O bond's rupture of CO_2 with a maximum at $2R_e$(C-O). Following both theoretical models, a strong structural transition takes place between the field-free geometry and the exploding nuclear configuration. This situation is specific to strong field effects in molecular physics and remains to be investigated in more detail using both improved experimental methods and theoretical developments.

The author is pleased to acknowledge P. d'Oliveira and P. Meynadier for operating the CEA/DRECAM laser system and M. Bougeard and E. Caprin for their skilled technical assistance.

[1] C. Cornaggia, M. Schmidt, and D. Normand, J. Phys. B **27**, L123 (1994), and references therein.
[2] C. Cornaggia, M. Schmidt, and D. Normand, Phys. Rev. A **51**, 1431 (1995), and references therein.
[3] J. H. Posthumus, L. J. Frasinski, A. J. Giles, and K. Codling, J. Phys. B **28**, L349 (1995).
[4] T. Seideman, M. Yu. Ivanov, and P. B. Corkum, Phys. Rev. Lett. **75**, 2819 (1995).
[5] K. C. Kulander, F. H. Mies, and K. J. Schafer, in *Super-Intense Laser-Atom Physics IV*, edited by H. G. Muller and M. V. Fedorov (Kluwer Academic, Amsterdam, 1996), p. 163.
[6] T. Zuo and A. D. Bandrauk, Phys. Rev. A **52**, 1 (1995).
[7] K. Codling and L. J. Frasinski, J. Phys. B **26**, 783 (1993), and references therein.
[8] W. C. Wiley and I. H. McLaren, Rev. Sci. Instrum. **26**, 1150 (1955).
[9] K. J. Schafer, Baorui Yang, L. F. DiMauro, and K. C. Kulander, Phys. Rev. Lett. **70**, 1599 (1993).
[10] P. B. Corkum, Phys. Rev. Lett. **71**, 1994 (1993).